TOPICAL REVIEW — Topological electronic states

Weak antilocalization and interaction-induced localization of Dirac and Weyl Fermions in topological insulators and semimetals*

Hai-Zhou Lu(卢海舟)[1] and Shun-Qing Shen(沈顺清)[2]

[1] Department of Physics, South University of Science and Technology of China, Shenzhen 518055, China
[2] Department of Physics, The University of Hong Kong, Pokfulam Road, Hong Kong, China

(Received 19 January 2016; published online 28 September 2016)

Weak localization and antilocalization are quantum transport phenomena that arise from the quantum interference in disordered metals. At low temperatures, they can give distinct temperature and magnetic field dependences in conductivity, allowing the symmetry of the system to be explored. In the past few years, they have also been observed in newly emergent topological materials, including topological insulators and topological semimetals. In contrast from the conventional electrons, in these new materials the quasiparticles are described as Dirac or Weyl fermions. In this article, we review our recent efforts on the theories of weak antilocalization and interaction-induced localization for Dirac and Weyl fermions in topological insulators and topological semimetals.

Keywords: localization, antilocalization, topological insulator, topological semimetal

PACS: 72.25.−b, 75.47.−m, 78.40.Kc **DOI:** 10.1088/1674-1056/25/11/117202

1. Introduction

Weak antilocalization is a transport phenomenon in the quantum diffusion regime in disordered metals.[1] The quantum diffusion in disordered metals can be defined by the mean free path ℓ and the phase coherence length ℓ_ϕ. The mean free path measures the average distance that an electron travels before its momentum is changed by elastic scattering from static scattering centers, while the phase coherence length measures the average distance that an electron can maintain its phase coherence. If the mean free path is much shorter than the system size and the phase coherence length, then the electrons suffer from scattering but can maintain their phase coherence. This is the quantum diffusive regime, in which the quantum interference between time-reversed scattering loops (see Fig. 1(a)) can give rise to a correction to the conductivity. The weak localization or weak antilocalization arises due to this correction in the conductivity in the quantum diffusive regime.

The phase coherence length is determined by inelastic scattering from electron–phonon coupling and interaction with other electrons. The inelastic scattering has to be suppressed significantly to make the phase coherence length much longer than the mean free path. Therefore, the quantum diffusion usually takes place at extremely low temperatures; e.g., below the liquid helium temperature. If the quantum interference correction is positive, then it gives a weak antilocalization correction to the conductivity and the conductivity goes up with decreasing temperature (see Fig. 1(b)). Because this correction requires time reversal symmetry, it can be suppressed by applying a magnetic field. One can then observe that the conductivity goes down with increasing magnetic field. This negative magnetoconductivity or positive magnetoresistivity is the more familiar signature of the weak antilocalization (see Fig. 1(c)).

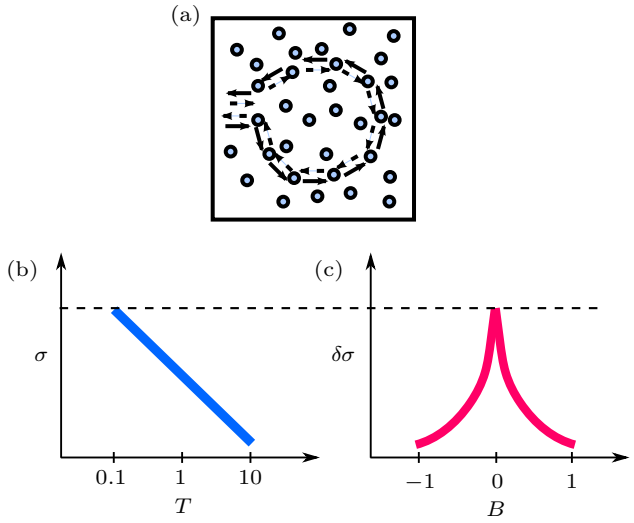


Fig. 1. (color online) (a) Schematic illustration of time-reversed scattering loops in the quantum diffusion regime in disordered metals. The open circles represent impurities and the arrows mark the trajectories that electrons travel. (b) and (c) The signatures of the weak antilocalization (WAL) in (b) temperature (T) dependence of the conductivity σ and (c) magnetoconductivity [defined as $\delta\sigma \equiv \sigma(B) - \sigma(0)$], where B is the magnetic field.

In contrast, the quantum interference can be negative, leading to a weak localization effect and totally opposite temperate and magnetic dependencies of conductivity. Whether a

*Project supported by the National Key R & D Program, China (Grant No. 2016YFA0301700), the Research Grant Council, University Grants Committee, Hong Kong, China (Grant No. 17303714), the National Natural Science Foundation of China (Grant No. 11574127), and the National Thousand-Young-Talents Program of China.

© 2016 Chinese Physical Society and IOP Publishing Ltd

system has weak localization or weak antilocalization depends on the symmetry (see Table 1). According to the classification of the ensembles of random matrix,[2] there are three symmetry classes. If a system has no time-reversal symmetry, then it is in the unitary class, in which there is no weak localization or antilocalization. If a system has time-reversal symmetry but no spin-rotational symmetry, then it is in the symplectic class, in which the weak antilocalization is expected. If a system has both time-reversal and spin-rotational symmetries, then it is in the orthogonal class, in which the weak localization is expected. These symmetry arguments have been well known since the studies on the conventional 2D electron gases.[3]

Table 1. The relation between the symmetry classes (orthogonal, symplectic, and unitary)[2] and the weak localization (WL) and antilocalization (WAL).[3]

	Orthogonal	Symplectic	Unitary
Time-reversal	√	√	×
Spin-rotational	√	×	×
WL/WAL	WL	WAL	×

In the last decade, weak antilocalization has been widely observed in topological materials, such as topological insulators[4–9] and topological semimetals,[10–13] in which the quasiparticles are described not by the Schrödinger equation but as Dirac fermions in the topological insulators and Weyl fermions in the topological semimetals. For Dirac fermions, the weak antilocalization has an alternative understanding based on the Berry phase argument. The Berry phase is a geometric phase collected in an adiabatic cyclic process.[14,15] Since studies on carbon nanotubes have begun, it has been found that massless Dirac fermions can collect a π Berry phase after circulating around the Fermi surface.[16] The π Berry phase induces a destructive quantum interference between time-reversed loops formed by scattering trajectories. The destructive interference can suppress backscattering of electrons, the conductivity is then enhanced with decreasing temperature because the decoherence mechanisms are suppressed at low temperatures.[17,18]

One of the powerful theoretical approaches to study weak localization and antilocalization is the Feynman diagram techniques. Figure 2 summarizes the Feynman diagrams we have used to study the weak localization and antilocalization arising from the quantum interference and interaction. Simply speaking, it is based on the linear response theory of the conductivity, with disorder and interaction taken as perturbations. In the formulism, there are three main contributions to the conductivity. The leading order is the semiclassical Drude conductivity (Fig. 2(a)), and then the quantum interference correction (Fig. 2(b)) and the interaction correction (Altshuler–Aronov effect) (Fig. 2(d)).

In this paper, we review our recent efforts[19–22] on the weak antilocalization and interaction-induced localization of Dirac and Weyl fermions in topological insulators and topological semimetals.[19–25] Part of the contents have been reviewed in Ref. [26], where only topological insulators are addressed. In Section 2, we discuss the Berry phase argument and the crossover between weak antilocalization and weak localization in magnetically modulated topological insulator and topological insulator thin films. In Section 3, we show the weak localization of Dirac fermions as a result of electron–electron interactions. In Section 4, we review the weak antilocalization and interaction-induced localization of Weyl fermions in 3D topological semimetals. Finally, remarks and perspective are given in Section 5.

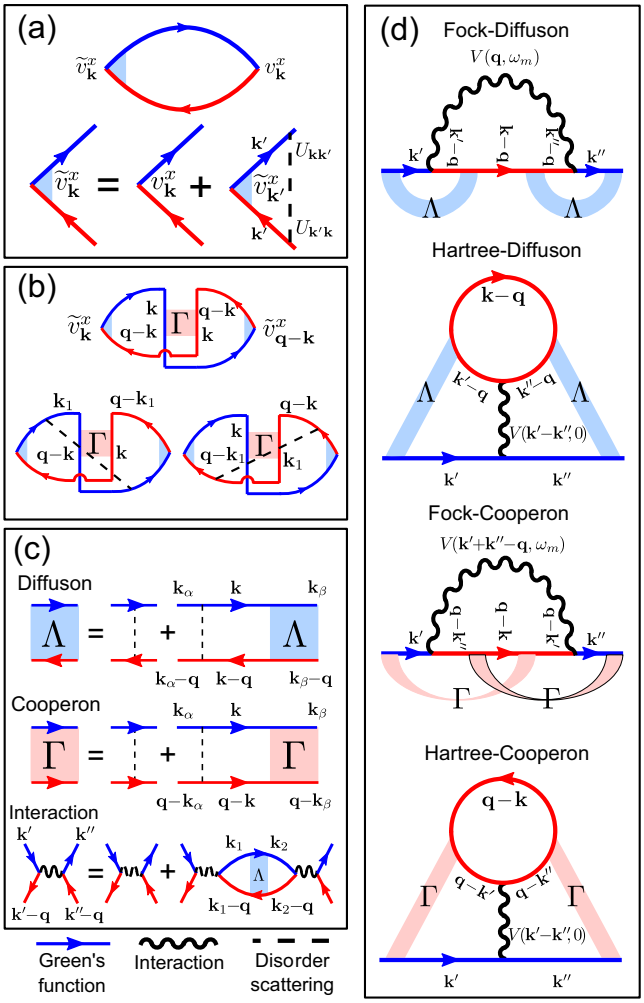


Fig. 2. (color online) (a) The diagrams for the semiclassical conductivity $\sigma^{\rm sc}$. v and $\tilde{v}$ are the bare velocity and the velocity after the vertex correction, respectively. (b) The Hikami boxes of the maximally-crossed diagrams, from which the conductivity correction from the quantum interference $\sigma^{\rm qi}$ is calculated.[18] (c) The iteration equations for the Diffuson (Λ), Cooperon (Γ), and dynamically screened interaction. (d) The Fock and Hartree self-energies dressed by Diffuson and Cooperon, from which the conductivity correction from the electron–electron interaction $\sigma^{\rm ee}$ is calculated. $\boldsymbol{k}$ and $\boldsymbol{q}$ stand for the wave vectors, and ε_n and ω_m for the Matsubara frequencies. Adapted from Ref. [19].

2. Weak antilocalization in topological insulators

Topological insulators are gapped band insulators with topologically protected gapless modes surrounding their boundaries.[4–9] The surface of a three-dimensional topological insulator hosts an odd number of two-dimensional gapless Dirac cones. The Dirac cone has a helical spin structure in momentum space.[27] The topological insulators have attracted tremendous interest in their transport properties.[28,29] It turns out that the known topological insulator materials all have poor mobility. The mean free path is of the order of 10 nm, while the phase coherence length can reach up to 100–1000 nm below the liquid helium temperature. In other words, these materials are well in the quantum diffusion regime at low temperatures, where the weak (anti-)localization is expected. In experiments, the negative magnetoconductivity arising from the weak antilocalization has been observed in almost every topological insulator sample.[30–39]

The surface states of a topological insulator can be described by a two-dimensional massless Dirac model

$$H = \gamma(\sigma_x k_y - \sigma_y k_x), \tag{1}$$

where γ is a parameter related to the effective velocity, $\boldsymbol{\sigma} = (\sigma_x, \sigma_y)$ are the Pauli matrices, and $\boldsymbol{k} = (k_x, k_y)$ is the wave vector. The model describes a conduction band and valence band touching at the Dirac point. Without loss of generality, we can focus on the conduction band. The spinor wavefunction of the conduction band is written as

$$\psi_{\boldsymbol{k}}(\boldsymbol{r}) = \frac{1}{\sqrt{2}} \begin{pmatrix} 1 \\ -\mathrm{i}\,\mathrm{e}^{\mathrm{i}\varphi} \end{pmatrix} \mathrm{e}^{\mathrm{i}\boldsymbol{k}\cdot\boldsymbol{r}}, \tag{2}$$

with $\tan\varphi = k_y/k_x$. The spinor wave function describes the helical spin structure of the surface states, which can give rise to a π Berry phase when an electron moves adiabatically around the Fermi surface.[40]

The Berry phase is a geometric phase collected in an adiabatic cyclic process,[15,16] and it can be found as

$$\phi_{\mathrm{b}} \equiv -\mathrm{i}\int_0^{2\pi} \mathrm{d}\varphi \left\langle \psi_{\boldsymbol{k}}(\boldsymbol{r}) \middle| \frac{\partial}{\partial\varphi} \middle| \psi_{\boldsymbol{k}}(\boldsymbol{r}) \right\rangle = \pi. \tag{3}$$

The π Berry phase can give an explanation of the weak antilocalization of the two-dimensional massless Dirac fermions. The time-reversed scattering loops in Fig. 1(a) are equivalent to moving an electron on the Fermi surface by one cycle. The Berry phase then plays an important role. The π Berry phase give rises to a destructive quantum interference that suppresses the back scattering and enhances the conductivity, leading to the weak antilocalization.[17,18] The π Berry phase can lead to the absence of backscattering,[41] and further the delocalization of the surface electron.[42,43]

To verify the role played by the Berry phase, one can alter the Berry phase by including a mass to the Dirac model[7,44]

$$H = \gamma(\sigma_x k_y - \sigma_y k_x) + \frac{\Delta}{2}\sigma_z. \tag{4}$$

Now the conduction and valence bands are separated by a gap Δ. With the mass term, the Berry phase turns out to be[20]

$$\phi_{\mathrm{b}} = \pi\left(1 - \frac{\Delta}{2E_{\mathrm{F}}}\right), \tag{5}$$

where the Fermi energy E_{F} is measured from the Dirac point. In the presence of the finite Δ, and if one moves the Fermi energy to the bottom of the conduction band, where $E_{\mathrm{F}} = \Delta/2$, the Berry phase becomes $\phi_{\mathrm{b}} = 0$. In this so-called large-mass limit, the quantum interference changes to constructive, resulting in the crossover to the weak localization.[20,45,46] The crossover from weak antilocalization to weak localization has been observed in many experiments, where the mass term may arise in several cases. The first one is the magnetically doped surface states.[47–49] In an earlier attempt, we showed that the sharp WAL magnetoconductivity can be completely suppressed by doping Fe on the top surface of the topological insulator Bi_2Te_3.[34] Later, a complete sign change in magnetoconductivity was observed in 3-quintuple-layer Cr-doped Bi_2Se_3,[50] Mn-doped Bi_2Se_3,[51] EuS/Bi_2Se_3 bilayers,[52] and $Sb_{1.9}Bi_{0.1}Te_3$ micro flakes grown on the ferrimagnet $BaFe_{12}O_{19}$.[53] The second is the finite-size effect of the surface states.[54] A WAL–WL crossover as a function of the gate voltage has been observed in a 4-quintuple-layer $Bi_{1.14}Sb_{0.86}Te_3$.[55] The third is the bulk states in a thin film of topological insulator.[21] The weak localization is quite different from that in other systems with strong spin–orbit interaction, where weak antilocalization is usually expected. This result was soon supported by other theoretical[56] and experimental works.[57,58]

3. Interaction-induced localization in topological insulators

An alternative definition of a topological insulator is that its topologically protected surface states cannot be localized.[4,5,42,43] The negative magnetoconductivity of the weak antilocalization has been regarded as a signature of this delocalization tendency. However, in most experiments, a suppression of the conductivity with decreasing temperature is observed (see Fig. 3),[35–37,60–62] showing a tendency of localization.[1,63] In other words, the experimental observation in magnetoconductivity and finite temperature conductivity presents a transport paradox in topological insulators.

The electron–electron interaction[64,65] provides a possible way to understand the contradictory magnetic field and temperature dependences.[19] The interplay of the interaction and disorder can lead to a temperature dependence much like the weak localization, known as the Altshulter–Aronov

effect.[64,65] The theory is established for conventional electrons. We show that Dirac fermions are not immune from the Altshuler–Aronov effect. With or without the magnetic field, the correction from the interaction to the conductivity decreases logarithmically with decreasing temperature. Although the weak antilocalization can enhance the conductivity with decreasing temperature, it is overwhelmed by the contribution from the interaction effect. Therefore, the overall temperature dependence of the conductivity shows a weak localization tendency. Our theoretical results agree well with the experiments, with comparable changes of the conductivity (several e^2/h), temperatures (0.1 to 10 K), and magnetic fields (0 to 5 T).[35–37,60–62]

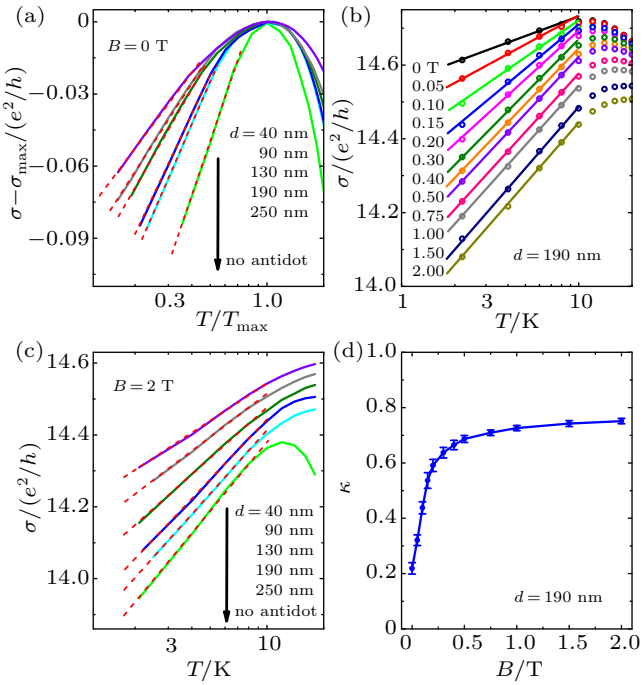


Fig. 3. (color online) (a) Measured logarithmic temperature-dependent conductivity (solid lines) at zero magnetic field for all samples with the edge-to-edge distance between antidots d indicated. The red dashed lines are guide for eyes. (b) Measured logarithmic temperature-dependent conductivity at indicating perpendicular magnetic fields (open circles) for sample $d190$. Solid lines are the linear fitting curves. (c) Measured temperature-dependent conductivity (solid lines) at $B = 2$ T for all samples with d indicated. The curves are offset for clarity and the red dashed lines are guide for eyes. (d) The slope obtained by linear fitting the curves in panel (b) is plotted (solid symbols) as a function of the magnetic field for sample $d190$. Solid lines are guide for eyes. Adapted from Ref. [59].

Furthermore, to verify the interaction effect, we proposed an artificial nanostructure[59] as shown in Fig. 4. The temperature dependence of the conductivity is characterized by the slope defined as

$$\kappa \equiv \frac{\pi h}{e^2}\frac{\partial \sigma}{\partial \ln T}. \tag{6}$$

In strong magnetic fields, the slope is solely determined by the interaction effect. As an interaction effect, the slope is supposed to be changed by changing the dielectric constant ε_r. We calculated the slope from the interaction κ^{ee} as a function of ε_r for the surface electrons as plotted in Fig. 5(a). One can see that κ^{ee} decreases monotonically with decreasing ε_r.

To modulate the dielectric constant, we fabricated an array of antidots arranged in a periodic triangular lattice in thin films of Bi_2Te_3, as schematically indicated in Fig. 4(a). The diameter of each antidot is fixed at 200 nm. The edge-to-edge distances d of two neighboring antidots are 40 nm, 90 nm, 130 nm, 190 nm, and 250 nm, respectively. A smaller value of d represents a larger density of antidots. The dielectric constant of Bi_2Te_3 is of the order of 10–100,[68] while that of the vacuum at the antidots is 1. According to the effective medium theory,[67] with decreasing distance between the antidots, i.e., more antidots, the dielectric constant is supposed to be reduced. As a result, the slope is also expected to decrease with decreasing distant between the antidots. This is consistent with the observation in Figs. 3 and 5.

In this way, we show that two-dimensional massless Dirac fermions can show the localization tendency when both the electron–electron interaction and disorder scattering are taken into account.

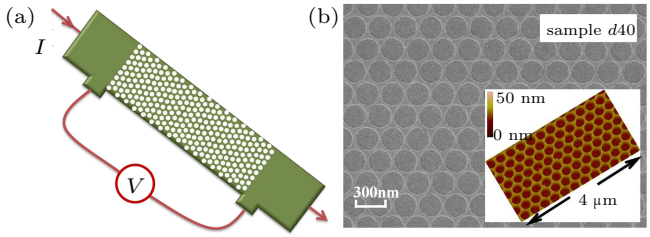


Fig. 4. (color online) (a) Schematic illustration of a Hall bar sample with antidot array. (b) Scanning electron microscopy image of a Bi_2Te_3 thin film with antidot array, where the edge-to-edge distance between antidots $d = 40$ nm. The inset is the atomic force microscope image indicating that the antidots depth is about 25 nm. Adapted from Ref. [59].

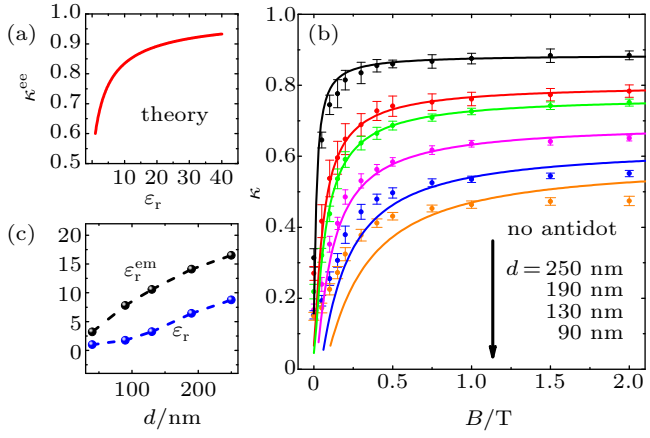


Fig. 5. (color online). (a) The calculated slope κ^{ee} as a function of relative dielectric constant ε_r for gapless Dirac fermions. $v\hbar$ is chosen to be 2.5 eV·Å, comparable with that in the experiment.[66] (b) The slope κ of the conductivity–ln$T$ curve as a function of magnetic field B for different antidot distance d. The measured κ (scatters) are fitted by the theory[19] (solid curves). (c) The dielectric constant as a function of d, obtained by fitting the transport theory (ε_r) and calculated from the Bruggeman effective medium theory (ε_r^{em}), respectively.[67] The intrinsic dielectric constant $\varepsilon_b = 22.0$ of the no-antidot sample is extracted by fitting the transport theory. Adapted from Ref. [59].

4. Weak antilocalization and interaction-induced localization in topological semimetals

Weyl semimetal is a three-dimensional (3D) topological state of matter, in which the conduction and valence energy bands touch at a finite number of nodes.[10] The nodes always appear in pairs, in each pair the quasiparticles (dubbed Weyl fermions) carry opposite chirality and linear dispersion, much like a 3D analog of graphene. In the past few years, a number of condensed matter systems have been suggested to host Weyl fermions.[11–13,70–78] Recently, angle-resolved photoemission spectroscopy (ARPES) has identified the Dirac nodes (doubly-degenerate Weyl nodes)[72] in $(Bi_{1-x}In_x)_2Se_3$,[79,80] Na_3Bi,[74,76,81,82] and Cd_3As_2[76,83–86] and Weyl nodes in the TaAs family.[87–91] The negative magnetoconductivity arising from the weak antilocalization has been observed recently in $Bi_{0.97}Sb_{0.03}$,[92,93] $ZrTe_5$,[94] and TaAs.[88,95]

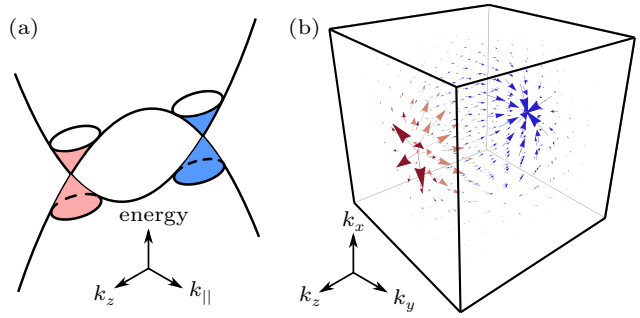


Fig. 6. (color online) Nontrivial band structure and Berry curvature of a topological semimetal. (a) A schematic of the energy spectrum of a topological semimetal. (k_x, k_y, k_z) is the wave vector. $k_{||}^2 = k_x^2 + k_y^2$. (b) The vector plot of the Berry curvature in momentum space. The conduction and valence bands of a topological semimetal touch at the Weyl nodes, at which a pair of monopoles are hosted. The arrows show that the flux of the Berry curvature flows from one monopole (red) to the other (blue), defining the nontrivial topological properties of the topological semimetal. Adapted from Ref. [69].

One of the low-energy descriptions of Weyl fermions in semimetals is

$$H = \pm\hbar v_{\rm F}\boldsymbol{\sigma}\cdot\boldsymbol{k}, \tag{7}$$

where the valley index $\pm$ describes the opposite chirality, $v_{\rm F}$ is the Fermi velocity, $\hbar$ is the reduced Planck constant, $\boldsymbol{\sigma} = (\sigma_x, \sigma_y, \sigma_z)$ is the vector of Pauli matrices, and $\boldsymbol{k}$ is the wave vector measured from the Weyl nodes at $\pm\boldsymbol{k}_{\rm c}$. Note that the model has the symplectic symmetry, so the weak antilocalization is expected. Moreover, we find the Berry phase can also explain the weak localization in Weyl semimetals.[25]

We calculate the magnetoconductivity arising from the quantum interference, as shown in Fig. 7. As $B \to 0$, $\delta\sigma^{\rm qi}$ is proportional to $-\sqrt{B}$ for $\ell_\phi \gg \ell_B$ or at low temperatures, and $\delta\sigma^{\rm qi} \propto -B^2$ for $\ell_\phi \ll \ell_B$ at high temperatures. ℓ_B can be evaluated approximately as $12.8/\sqrt{B}$ nm with B in units of Tesla. Usually, below the liquid helium temperature ℓ_ϕ can be as long as hundreds of nanometers to one micrometer, much longer than ℓ_B, which is tens of nanometers between 0.1 T and 1 T. Therefore, the $-\sqrt{B}$ magnetoconductivity at low temperatures and small fields serves as a signature for the weak antilocalization of 3D Weyl fermions. Figure 7(a) shows $\delta\sigma^{\rm qi}(B)$ of two valleys of Weyl fermions in the absence of intervalley scattering. For long ℓ_ϕ, $\delta\sigma^{\rm qi}(B)$ is negative and proportional to $\sqrt{B}$, showing the signature of the weak antilocalization of 3D Weyl fermions. This $-\sqrt{B}$ dependence agrees well with the experiment,[92,93] and we emphasize that it is obtained from a complete diagram calculation with only two parameters ℓ and ℓ_ϕ of physical meanings. As ℓ_ϕ becomes shorter, a change from $-\sqrt{B}$ to $-B^2$ is evident. $\delta^{\rm qi}(B)$ vanishes at $\ell_\phi = \ell$ as the system quits the quantum interference regime.

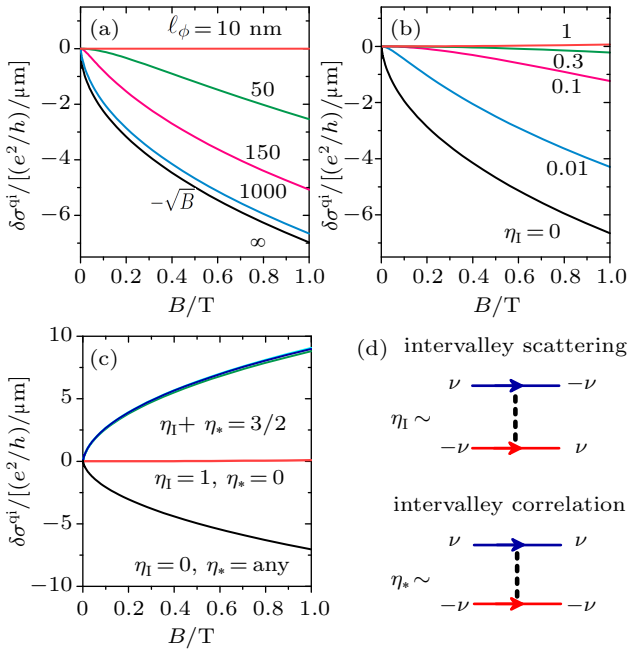


Fig. 7. (color online) The magnetoconductivity $\delta\sigma^{\rm qi}(B)$ for different phase coherence length ℓ_ϕ at $\eta_{\rm I} = \eta_* = 0$ (a), for different $\eta_{\rm I}$ at $\eta_* = 0$ (b), and for different $\eta_{\rm I}$ at finite η_* (c). The magnetic field B is applied along arbitrary directions. Parameters $\ell = 10$ nm and $\ell_\phi = 1000$ nm in panels (b) and (c). (d) The diagrams show the difference between $\eta_{\rm I}$ and η_*, with $\eta_{\rm I}$ related to the intervalley scattering and η_* measuring the intervalley correlation of intravalley scattering. The dashed lines represent the correlation of two scattering processes. $\nu = \pm$ is the valley index. Adapted from Ref. [24].

Based on the theory in Ref. [24], we proposed a formula to fit the magnetoconductivity arising from the weak localization, and it has been applied in the experiment on TaAs[95]

$$\delta\sigma(B) = -C_{\rm WAL}\left(\sqrt{B}\frac{B^2}{B^2+B_{\rm c}^2} + \gamma B^2\frac{B_{\rm c}^2}{B^2+B_{\rm c}^2}\right), \tag{8}$$

where the fitting parameters $C_{\rm WAL}$ and γ are positive and the critical field $B_{\rm c}$ is related to the phase coherence length ℓ_ϕ, i.e., $B_{\rm c} \sim \hbar/e\ell_\phi^2$. Empirically, the phase coherence length becomes longer with decreasing temperature and can be written as $\ell_\phi \sim T^{-p/2}$; then $B_{\rm c} \sim T^p$, where p is positive and determined by decoherence mechanisms such as electron–electron

interaction ($p = 3/2$) or electron–phonon interaction ($p = 3$). At high temperatures, $\ell_\phi \to 0$; thus, $B_c \to \infty$ and we have $\delta\sigma_{zz}^{qi} \propto B^2$. At low temperatures, $\ell_\phi \to \infty$; then $B_c = 0$ and we have $\delta\sigma_{zz}^{qi} \propto \sqrt{B}$. By fitting the magnetoconductivity, we find that $p \approx 1.5$.[95]

In the presence of the interaction, we find that the change of conductivity with temperature for one valley of Weyl fermions can be summarized as

$$\Delta\sigma(T) = c_{ee}T^{1/2} - c_{qi}T^{p/2}, \tag{9}$$

where both c_{ee} and c_{qi} are positive parameters. This describes a competition between the interaction-induced weak localization and the interference-induced weak antilocalization, as shown in Fig. 8 schematically. At higher temperatures, the conductivity increases with decreasing temperature, showing a weak antilocalization behavior. Below a critical temperature T_c, the conductivity starts to drop with decreasing temperature, exhibiting a localization tendency. The critical temperature can be found as $T_c = \left(c_{ee}/p \cdot c_{qi}\right)^{2/(p-1)}$. Because $c_{ee}, c_{qi} > 0$, this means as long as $p > 1$, there is always a critical temperature below which the conductivity drops with decreasing temperature. For known decoherence mechanisms in 3D, p is always greater than 1.[1] With a set of typical parameters, we find that $T_c \approx 0.4$–10^6 K.[24]

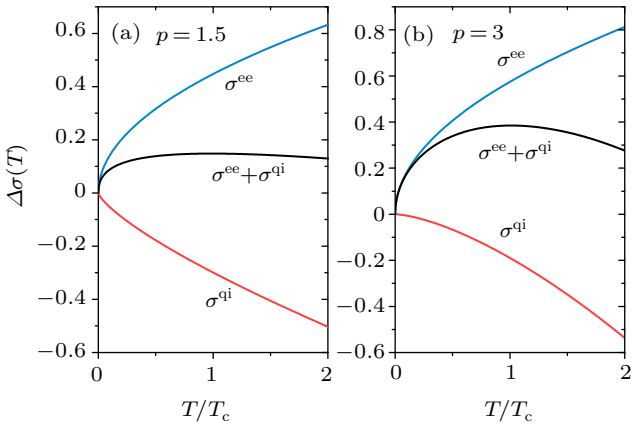


Fig. 8. (color online) A schematic demonstration of the change of conductivity $\Delta\sigma$ as a function of temperature T. We choose $c_{ee} = c_{qi}$. T_c is the critical temperature below which the conductivity drops with decreasing temperature. Adapted from Ref. [24].

We find that the intervalley scattering and correlation can also lead to the weak localization. Two dimensionless parameters are defined for the inter- and intravalley scattering: $\eta_* \propto \langle U^{++}_{\boldsymbol{k},\boldsymbol{k}'} U^{--}_{\boldsymbol{k}',\boldsymbol{k}} \rangle$ measuring the correlation between intravalley scattering and $\eta_I \propto \langle U^{+-}_{\boldsymbol{k},\boldsymbol{k}'} U^{-+}_{\boldsymbol{k}',\boldsymbol{k}} \rangle$ measuring the weight of intervalley scattering , where $U^{\nu,\nu'}_{\boldsymbol{k},\boldsymbol{k}'}$ is the scattering matrix element. Figure 7(d) schematically shows the difference between η_* and η_I. As shown in Fig. 7(b), with increasing η_I, the negative $\delta\sigma^{qi}$ is suppressed, where $\eta_I \to 1$ means strong intervalley scattering while $\eta_I \to 0$ means vanishing intervalley scattering. Furthermore, figure 7(c) shows that the magnetoconductivity can turn to positive when $\eta_I + \eta_* = 3/2$. The positive $\delta\sigma^{qi}(B)$ in Fig. 7(c) corresponds to a suppressed σ^{qi} with decreasing temperature, i.e., a localization tendency. This localization is attributed to the strong intervalley coupling which recovers spin-rotational symmetry (now the spin space is complete for a given momentum), the system then goes to the orthogonal class.[2,3,17] Therefore, we show that the combination of strong intervalley scattering and correlation will strengthen the localization tendency in disordered Weyl semimetals.

5. Remarks and Perspective

In summary, we systematically studied the weak antilocalization and interaction-induced localization for Dirac and Weyl fermions in topological insulators and topological semimetals. With the help of Feynman diagram techniques, we considered the correction to the conductivity from the quantum interference correction and electron–electron interaction. We predicted the crossover between weak antilocalization and weak localization for the massive Dirac fermions. The theory can be applied to magnetically doped topological insulators and surface and bulk states in topological insulator thin films. With the help of an antidot nanostructure in topological insulator thin films, we verified the interaction induced localization tendency for Dirac fermions in topological insulators. We also studied the weak antilocalization and interaction effect in Weyl semimetals. For a single valley of Weyl fermions, we found that the magnetoconductivity is negative and proportional to the square root of the magnetic field at low temperatures, giving the signature for the weak antilocalization in three dimensions as well as for the Weyl fermion. In the presence of strong intervalley effects, we expected a crossover from the weak antilocalization to weak localization. In addition, we found that the interplay of electron–electron interaction and disorder scattering can also give rise to a tendency to localization for Weyl fermions.

Finally, we remark on the possible future works. On the weak localization induced by the interaction, the bulk and surface states still coexist on the Fermi surface in the latest experiment work. To show the interaction-induced localization of the surface states, further experiments are still needed to be performed in intrinsic topological insulators by doping[96] or using ternary and quaternary compounds.[97–103] Topological Weyl semimetals provide a new platform to study the weak antilocalization in three dimensions. Our formula of magnetoconductivity can be used for a systematic study of the transport experiments on topological semimetals. One of the interesting fields is the theories of the weak localization for semimetals with monopole charges higher than 1, as has recently been explored for the double-Weyl semimetals.[25] Also, the weak (anti-)localization theories for nodal-line and

drumhead semimetal could be interesting topics for further research.

Acknowledgments

We thank fruitful discussions with our collaborators Junren Shi, Jiannong Wang, Fuchun Zhang, Michael Ma, Hongtao He, Wenyu Shan, Songbo Zhang, Hongchao Liu, Hui Li, Guolin Zheng, and Mingliang Tian.

References

[1] Lee P A and Ramakrishnan T V 1985 *Rev. Mod. Phys.* **57** 287
[2] Dyson F J 1962 *J. Math. Phys.* **3** 140
[3] Hikami S, Larkin A I and Nagaoka Y 1980 *Progr. Theor. Phys.* **63** 707
[4] Moore J E 2010 *Nature* **464** 194
[5] Hasan M Z and Kane C L 2010 *Rev. Mod. Phys.* **82** 3045
[6] Qi X L and Zhang S C 2011 *Rev. Mod. Phys.* **83** 1057
[7] Shen S Q 2012 *Topological Insulators* (Berlin Heidelberg: Springer-Verlag)
[8] Ando Y 2013 *J. Phys. Soc. Jpn.* **82** 102001
[9] Yan B and Zhang S C 2012 *Rep. Prog. Phys.* **75** 096501
[10] Balents L 2011 *Physics* **4** 36
[11] Wan X, Turner A M, Vishwanath A and Savrasov S Y 2011 *Phys. Rev. B* **83** 205101
[12] Yang K Y, Lu Y M and Ran Y 2011 *Phys. Rev. B* **84** 075129
[13] Burkov A A and Balents L 2011 *Phys. Rev. Lett.* **107** 127205
[14] Pancharatnam S 1956 *Proc. Indian Acad. Sci. A* **44** 247
[15] Berry M V 1984 *Proc. R. Soc. A* **392** 45
[16] Shon N H and Ando T 1998 *J. Phys. Soc. Jpn.* **67** 2421
[17] Suzuura H and Ando T 2002 *Phys. Rev. Lett.* **89** 266603
[18] McCann E, Kechedzhi K, Fal'ko V I, Suzuura H, Ando T and Altshuler B L 2006 *Phys. Rev. Lett.* **97** 146805
[19] Lu H Z and Shen S Q 2014 *Phys. Rev. Lett.* **112** 146601
[20] Lu H Z, Shi J and Shen S Q 2011 *Phys. Rev. Lett.* **107** 076801
[21] Lu H Z and Shen S Q 2011 *Phys. Rev. B* **84** 125138
[22] Shan W Y, Lu H Z and Shen S Q 2012 *Phys. Rev. B* **86** 125303
[23] Lu H Z, Yao W, Xiao D and Shen S Q 2013 *Phys. Rev. Lett.* **110** 016806
[24] Lu H Z and Shen S Q 2015 *Phys. Rev. B* **92** 035203
[25] Dai X, Lu H Z, Shen S Q and Yao H 2016 *Phys. Rev. B* **93** 161110(R)
[26] Lu H Z and Shen S Q 2014 *Proc. SPIE 9167, Spintronics VII, 91672E*
[27] Xia Y, Qian D, Hsieh D, Wray L, Pal A, Lin H, Bansil A, Grauer D, Hor Y S, Cava R J and Hasan M Z 2009 *Nat. Phys.* **5** 398
[28] Culcer D 2012 *Physica E* **44** 860
[29] Bardarson J H and Moore J E 2013 *Reports on Progress in Physics* **76** 056501
[30] Checkelsky J G, Hor Y S, Liu M H, Qu D X, Cava R J and Ong N P 2009 *Phys. Rev. Lett.* **103** 246601
[31] Peng H, Lai K, Kong D, Meister S, Chen Y, Qi X L, Zhang S C, Shen Z X and Cui Y 2010 *Nat. Mater.* **9** 225
[32] Chen J, Qin H J, Yang F, Liu J, Guan T, Qu F M, Zhang G H, Shi J R, Xie X C, Yang C L, Wu K H, Li Y Q and Lu L 2010 *Phys. Rev. Lett.* **105** 176602
[33] Checkelsky J G, Hor Y S, Cava R J and Ong N P 2011 *Phys. Rev. Lett.* **106** 196801
[34] He H T, Wang G, Zhang T, Sou I K, Wong G K L, Wang J N, Lu H Z, Shen S Q and Zhang F C 2011 *Phys. Rev. Lett.* **106** 166805
[35] Liu M, Chang C Z, Zhang Z, Zhang Y, Ruan W, He K, Wang L l, Chen X, Jia J F, Zhang S C, Xue Q K, Ma X and Wang Y 2011 *Phys. Rev. B* **83** 165440
[36] Wang J, DaSilva A M, Chang C Z, He K, Jain J K, Samarth N, Ma X C, Xue Q K and Chan M H W 2011 *Phys. Rev. B* **83** 245438
[37] Chen J, He X Y, Wu K H, Ji Z Q, Lu L, Shi J R, Smet J H and Li Y Q 2011 *Phys. Rev. B* **83** 241304
[38] Kim Y S, Brahlek M, Bansal N, Edrey E, Kapilevich G A, Iida K, Tanimura M, Horibe Y, Cheong S W and Oh S 2011 *Phys. Rev. B* **84** 073109
[39] Steinberg H, Laloë J B, Fatemi V, Moodera J S and Jarillo-Herrero P 2011 *Phys. Rev. B* **84** 233101
[40] Shen S Q 2004 *Phys. Rev. B* **70** 081311
[41] Ando T, Nakanishi T and Saito R 1998 *J. Phys. Soc. Jpn.* **67** 2857
[42] Bardarson J H, Tworzydło J, Brouwer P W and Beenakker C W J 2007 *Phys. Rev. Lett.* **99** 106801
[43] Nomura K, Koshino M and Ryu S 2007 *Phys. Rev. Lett.* **99** 146806
[44] Shen S Q, Shan W Y and Lu H Z 2011 *SPIN* **01** 33
[45] Imura K I, Kuramoto Y and Nomura K 2009 *Phys. Rev. B* **80** 085119
[46] Ghaemi P, Mong R S K and Moore J E 2010 *Phys. Rev. Lett.* **105** 166603
[47] Hor Y S, Roushan P, Beidenkopf H, Seo J, Qu D, Checkelsky J G, Wray L A, Hsieh D, Xia Y, Xu S Y, Qian D, Hasan M Z, Ong N P, Yazdani A and Cava R J 2010 *Phys. Rev. B* **81** 195203
[48] Chen Y L, Chu J H, Analytis J G, Liu Z K, Igarashi K, Kuo H H, Qi X L, Mo S K, Moore R G, Lu D H, Hashimoto M, Sasagawa T, Zhang S C, Fisher I R, Hussain Z and Shen Z X 2010 *Science* **329** 659
[49] Wray L A, Xu S Y, Xia Y, Hsieh D, Fedorov A V, Hor Y S, Cava R J, Bansil A, Lin H and Hasan M Z 2011 *Nat. Phys.* **7** 32
[50] Liu M, Zhang J, Chang C Z, Zhang Z, Feng X, Li K, He K, Wang L l, Chen X, Dai X, Fang Z, Xue Q K, Ma X and Wang Y 2012 *Phys. Rev. Lett.* **108** 036805
[51] Zhang D, Richardella A, Rench D W, Xu S Y, Kandala A, Flanagan T C, Beidenkopf H, Yeats A L, Buckley B B, Klimov P V, Awschalom D D, Yazdani A, Schiffer P, Hasan M Z and Samarth N 2012 *Phys. Rev. B* **86** 205127
[52] Yang Q I, Dolev M, Zhang L, Zhao J, Fried A D, Schemm E, Liu M, Palevski A, Marshall A F, Risbud S H and Kapitulnik A 2013 *Phys. Rev. B* **88** 081407
[53] Zheng G, Wang N, Yang J, Wang W, Du H, Ning W, Yang Z, Lu H Z, Zhang Y and Tian M 2016 *Sci. Rep.* **6** 21334
[54] Lu H Z, Shan W Y, Yao W, Niu Q and Shen S Q 2010 *Phys. Rev. B* **81** 115407
[55] Lang M, He L, Kou X, Upadhyaya P, Fan Y, Chu H, Jiang Y, Bardarson J H, Jiang W, Choi E S, Wang Y, Yeh N C, Moore J and Wang K L 2013 *Nano Lett.* **13** 48
[56] Garate I and Glazman L 2012 *Phys. Rev. B* **86** 035422
[57] Zhang L, Dolev M, Yang Q I, Hammond R H, Zhou B, Palevski A, Chen Y and Kapitulnik A 2013 *Phys. Rev. B* **88** 121103
[58] Zhang H B, Yu H L, Bao D H, Li S W, Wang C X and Yang G W 2012 *Phys. Rev. B* **86** 075102
[59] Liu H C, Lu H Z, He H T, Li B, Liu S G, He Q L, Wang G, Sou I K, Shen S Q and Wang J 2014 *ACS Nano* **8** 9616
[60] Takagaki Y, Jenichen B, Jahn U, Ramsteiner M and Friedland K J 2012 *Phys. Rev. B* **85** 115314
[61] Chiu S P and Lin J J 2013 *Phys. Rev. B* **87** 035122
[62] Roy A, Guchhait S, Sonde S, Dey R, Pramanik T, Rai A, Movva H C P, Colombo L and Banerjee S K 2013 *Appl.Phys. Lett.* **102** 163118
[63] Bergmann G 1984 *Phys. Rep.* **107** 1
[64] Altshuler B L, Aronov A G and Lee P A 1980 *Phys. Rev. Lett.* **44** 1288
[65] Fukuyama H 1980 *J. Phys. Soc. Jpn.* **48** 2169
[66] Chen Y L, Analytis J G, Chu J H, Liu Z K, Mo S K, Qi X L, Zhang H J, Lu D H, Dai X, Fang Z, Zhang S C, Fisher I R, Hussain Z and Shen Z X 2009 *Science* **325** 178
[67] Aspnes D E 1982 *Am. J. Phys.* **50** 704
[68] Richter W and Becker C R 1977 *Physica Status Solidi* **84** 619
[69] Li H, He H T, Lu H Z, Zhang H C, Liu H C, Ma R, Fan Z Y, Shen S Q and Wang J N 2016 *Nat. Commun.* **7** 10301
[70] Delplace P, Li J and Carpentier D 2012 *Europhys. Lett.* **97** 67004
[71] Jiang J H 2012 *Phys. Rev. A* **85** 033640
[72] Young S M, Zaheer S, Teo J C Y, Kane C L, Mele E J and Rappe A M 2012 *Phys. Rev. Lett.* **108** 140405
[73] Xu G, Weng H M, Wang Z J, Dai X and Fang Z 2011 *Phys. Rev. Lett.* **107** 186806
[74] Wang Z, Sun Y, Chen X Q, Franchini C, Xu G, Weng H, Dai X and Fang Z 2012 *Phys. Rev. B* **85** 195320
[75] Singh B, Sharma A, Lin H, Hasan M Z, Prasad R and Bansil A 2012 *Phys. Rev. B* **86** 115208
[76] Wang Z, Weng H, Wu Q, Dai X and Fang Z 2013 *Phys. Rev. B* **88** 125427
[77] Liu J and Vanderbilt D 2014 *Phys. Rev. B* **90** 155316
[78] Bulmash D, Liu C X and Qi X L 2014 *Phys. Rev. B* **89** 081106
[79] Brahlek M, Bansal N, Koirala N, Xu S Y, Neupane M, Liu C, Hasan M Z and Oh S 2012 *Phys. Rev. Lett.* **109** 186403

[80] Wu L, Brahlek M, Valdes A R, Stier A V, Morris C M, Lubashevsky Y, Bilbro L S, Bansal N, Oh S and Armitage N P 2013 *Nat. Phys.* **9** 410
[81] Liu Z K, Zhou B, Zhang Y, Wang Z J, Weng H M, Prabhakaran D, Mo S K, Shen Z X, Fang Z, Dai X, Hussain Z and Chen Y L 2014 *Science* **343** 864
[82] Xu S Y, Liu C, Kushwaha S K, Sankar R, Krizan J W, Belopolski I, Neupane M, Bian G, Alidoust N, Chang T R, Jeng H T, Huang C Y, Tsai W F, Lin H, Shibayev P P, Chou F C, Cava R J and Hasan M Z 2015 *Science* **347** 294
[83] Liu Z K, Jiang J, Zhou B, Wang Z J, Zhang Y, Weng H M, Prabhakaran D, Mo S K, Peng H, Dudin P, Kim T, Hoesch M, Fang Z, Dai X, Shen Z X, Feng D L, Hussain Z and Chen Y L 2014 *Nat. Mater.* **13** 677
[84] Neupane M, Xu S Y, Sankar R, Alidoust N, Bian G, Liu C, Belopolski I, Chang T R, Jeng H T, Lin H, Bansil A, Chou F and Hasan M Z 2014 *Nat. Commun.* **5** 3786
[85] Yi H, Wang Z, Chen C, Shi Y, Feng Y, Liang A, Xie Z, He S, He J, Peng Y, Liu X, Liu Y, Zhao L, Liu G, Dong X, Zhang J, Nakatake M, Arita M, Shimada K, Namatame H, Taniguchi M, Xu Z, Chen C, Dai X, Fang Z and Zhou X J 2014 *Sci. Rep.* **4** 6106
[86] Borisenko S, Gibson Q, Evtushinsky D, Zabolotnyy V, Büchner B and Cava R J 2014 *Phys. Rev. Lett.* **113** 027603
[87] Weng H M, Fang C, Fang Z, Bernevig B A and Dai X 2015 *Phys. Rev. X* **5** 011029
[88] Huang S M, Xu S Y, Belopolski I, Lee C C, Chang G, Wang B K, Alidoust N, Bian G, Neupane M, Zhang C, Jia S, Bansil A, Lin H and Hasan M Z 2015 *Nat. Commun.* **6** 7373
[89] Lv B Q, Weng H M, Fu B B, Wang X P, Miao H, Ma J, Richard P, Huang X C, Zhao L X, Chen G F, Fang Z, Dai X, Qian T and Ding H 2015 *Phys. Rev. X* **5** 031013
[90] Xu S Y, Belopolski I, Alidoust N, Neupane M, Bian G, Zhang C L, Sankar R, Chang G Q, Yuan Z J, Lee C C, Huang S M, Zheng H, Ma J, Sanchez D S, Wang B K, Bansil A, Chou F C, Shibayev P P, Lin H, Jia S and Hasan M Z 2015 *Science* **349** 613
[91] Shekhar C, Nayak A K, Sun Y, Schmidt M, Nicklas M, Leermakers I, Zeitler U, Schnelle W, Grin J, Felser C and Yan B 2015 *Nat. Phys.* **11** 645
[92] Kim H J, Kim K S, Wang J F, Sasaki M, Satoh N, Ohnishi A, Kitaura M, Yang M and Li L 2013 *Phys. Rev. Lett.* **111** 246603
[93] Kim K S, Kim H J and Sasaki M 2014 *Phys. Rev. B* **89** 195137
[94] Li Q, Kharzeev D E, Zhang C, Huang Y, Pletikosic I, Fedorov A V, Zhong R D, Schneeloch J A, Gu G D and Valla T 2016 *Nature Physics Advance Online Publication*
[95] Zhang C, Xu S Y, Belopolski I, Yuan Z, Lin Z, Tong B, Alidoust N, Lee C C, Huang S M, Chang T R, Jeng H T, Lin H, Neupane M, Sanchez D S, Zheng H, Bian G, Wang J, Zhang C, Lu H Z, Shen S Q, Neupert T, Hasan M Z and Jia S 2016 *Nat. Commun.* **7** 10735
[96] Lang M, He L, Xiu F, Yu X, Tang J, Wang Y, Kou X, Jiang W, Fedorov A V and Wang K L 2012 *ACS Nano* **6** 295
[97] Xiong J, Petersen A, Qu D, Hor Y, Cava R and Ong N 2012 *Physica E* **44** 917
[98] Bao L, He L, Meyer N, Kou X, Zhang P, Chen Z g, Fedorov A V, Zou J, Riedemann T M, Lograsso T A, Wang K L, Tuttle G and Xiu F 2012 *Sci. Rep.* **2** 726
[99] Li Z, Chen T, Pan H, Song F, Wang B, Han J, Qin Y, Wang X, Zhang R, Wan J, Xing D and Wang G 2012 *Sci. Rep.* **2** 595
[100] Xia B, Ren P, Sulaev A, Liu P, Shen S Q and Wang L 2013 *Phys. Rev. B* **87** 085442
[101] Lee J, Park J, Lee J H, Kim J S and Lee H J 2012 *Phys. Rev. B* **86** 245321
[102] Jia S, Ji H, Climent-Pascual E, Fuccillo M K, Charles M E, Xiong J, Ong N P and Cava R J 2011 *Phys. Rev. B* **84** 235206
[103] Ren Z, Taskin A A, Sasaki S, Segawa K and Ando Y 2010 *Phys. Rev. B* **82** 241306